Mobility of Holstein Polaron at Finite Temperature: An Unbiased Approach

A. S. Mishchenko,[1,2] N. Nagaosa,[1,3] G. De Filippis,[4] A. de Candia,[4,5] and V. Cataudella[4]
[1]RIKEN Center for Emergent Matter Science (CEMS), 2-1 Hirosawa, Wako, Saitama 351-0198, Japan
[2]NRC "Kurchatov Institute", 123182 Moscow, Russia
[3]Department of Applied Physics, The University of Tokyo, 7-3-1 Hongo, Bunkyo-ku, Tokyo 113, Japan
[4]SPIN-CNR and Dipartimento di Fisica, Università di Napoli Federico II, I-80126 Napoli, Italy
[5]INFN, Sezione di Napoli, Complesso Universitario di Monte S. Angelo, I-80126 Napoli, Italy
(Received 25 June 2014; published 7 April 2015)

We present the first unbiased results for the mobility μ of a one-dimensional Holstein polaron obtained by numerical analytic continuation combined with diagrammatic and worldline Monte Carlo methods in the thermodynamic limit. We have identified for the first time several distinct regimes in the λ-T plane including a band conduction region, incoherent metallic region, an activated hopping region, and a high-temperature saturation region. We observe that although mobilities and mean free paths at different values of λ differ by many orders of magnitude at small temperatures, their values at T larger than the bandwidth become very close to each other.

DOI: 10.1103/PhysRevLett.114.146401 PACS numbers: 71.38.-k, 02.70.Ss, 72.20.Fr

Introduction.—The motion of a quantum particle in a background of quantum phonons (polaron) is an issue of fundamental importance [1]. Historically, it is the first condensed-matter problem where the quantum field theory has been successfully applied [2]. Experimentally, a small number of carriers in insulators and semiconductors introduced by doping or excited by light are key players in many important phenomena, where the transport properties of these carriers are influenced by polaron effects [3]. This is also the case of doped Mott insulators where the role of electron-phonon coupling (EPC) has to be considered in relation to high-temperature superconductivity [4].

There is no exact solution of the polaron problem and most of the analysis is based on approximate methods [1], ranging from variational [5] and perturbative approaches [6] to the momentum average approximation for the Green's function [7]. It is only recently that numerically exact solutions for the ground-state energy and optical conductivity at zero temperature were obtained by diagrammatic Monte Carlo simulations [8–13], variational [14–16] and exact [17] diagonalization, density-matrix renormalization group [18], and Chebyshev expansion [19], showing the limits of the different approximate schemes. Finite temperature properties are even more difficult to analyze due to several technical problems, and more than 6 decades of efforts to understand the temperature dependence of polaron mobility $\mu_\lambda(\omega, T)$, ranging from already historic papers [2,20–27] to the modern studies [3,28–35], established different behaviors which, however, do not exhaust the regimes exhibited by materials where EPC is relevant. To discuss them, we consider the one-dimensional Holstein polaron model [20]

$$\mathcal{H} = \sum_k (\varepsilon_k c_k^\dagger c_k + \omega_0 b_k^\dagger b_k) + \frac{g}{\sqrt{N}} \sum_{k,q} c_{k-q}^\dagger c_k (b_q^\dagger + b_{-q}).$$

Here, $c_k^\dagger$ ($b_k^\dagger$) are electron (phonon) creation operators in the state of momentum k. The dispersion $\varepsilon_{\mathbf{k}} = -2t\cos(ka)$ stems from a nearest-neighbor hopping on a linear lattice with lattice constant a, and the Einstein optical phonons have energy ω_0. The last term describes the local EPC. All sums over momenta are over the Brillouin zone, and we take the total number of sites $N \to \infty$. The charge current operator of the model is $\hat{j} = 2eat\sum_k \sin(ka) c_k^\dagger c_k$, where e is the electron charge. The strength of the EPC is measured by the dimensionless coupling constant $\lambda = g^2/(2t\omega_0)$, which sets the borderline between the weak- and strong-coupling regime at λ_c of the order of unity. For one polaron, we introduce the dynamic mobility $\mu_\lambda(\omega, T) = \sigma_\lambda(\omega, T)/e$ as a quantity related to the optical conductivity (OC) $\sigma_\lambda(\omega, T)$. The static mobility $\mu_\lambda(T) = \mu_\lambda(\omega \to 0, T)$ is just the quantity measured in standard transport experiments.

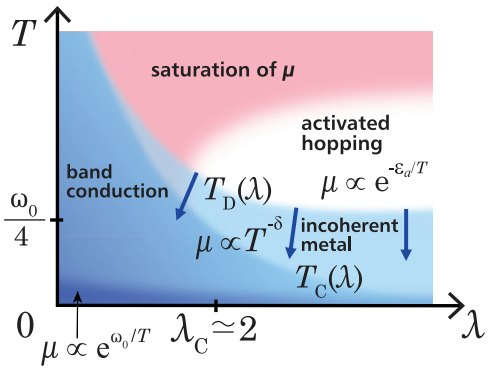

FIG. 1 (color online). Transport regimes of polaron. Schematic phase diagram showing the four different regimes of polaron mobility μ in the plane of λ-T (λ: EPC strength, T: temperature). Here, the unit of energy is $t = 1$, and ω_0 is the phonon frequency. Arrows show the direction of shift of the borderlines between different regimes when the phonon frequency decreases.

The phase diagram.—In Fig. 1 the different transport regions, emerging in the λ-T plane, are highlighted [36]. The optical conductivity is obtained through analytic continuation, starting from the current-current correlation function, calculated with diagrammatic and worldline Monte Carlo methods and by using a stochastic optimization approach (see the Supplemental Material [37]). As was revealed from our numeric results, there are two main crossovers separating distinct regions. One is the temperature $T_D(\lambda)$ above which the Drude-like peak (DLP) in $\mu_\lambda(\omega, T)$ disappears. The second is the temperature $T_C(\lambda)$ above which the mean free path (MFP) becomes shorter than the lattice constant. We found that $T_D(\lambda)$ coincides with the change in the temperature dependence of $\mu_\lambda(T)$, while $T_C(\lambda)$ indicates the crossover from the *band conduction* to the *incoherent metallic* motion. Namely, despite an always metallic T dependence $d\mu_\lambda(T)/dT < 0$ at $T < T_D(\lambda)$, one cannot always assume that the description in terms of a standard band motion with large MFP is valid. Indeed, the band motion takes place only in the left lower corner of the λ-T diagram, whereas the incoherent metallic behavior with short MFP is realized at $T > T_C(\lambda)$. Note the absolutely different nature of transport in these two regimes that both display power-law T dependence

$$\mu_{\text{metal}}(T) \sim T^{-\delta} \tag{1}$$

with the index $\delta \approx 2$ at weak ($\lambda \ll 1$) and $\delta \approx 3$ at intermediate and strong couplings ($\lambda \geq 0.5$).

As raising T above $T_D(\lambda)$, the temperature dependence of mobility $\mu_\lambda(T)$ considerably changes. At high temperatures "mobility saturation" is observed: the steepness of the mobility temperature dependence $d\mu_\lambda(T)/dT$ becomes considerably smaller for weak EPC $\lambda < \lambda_c$. In contrast, at larger EPC, $\lambda > \lambda_c$, and lower temperatures [but still at $T > T_D(\lambda)$], a different transport regime, the well-known "activated hopping," sets in: $d\mu_\lambda(T)/dT$ becomes positive. It has been derived analytically [20,21,25,31,46] and confirmed for specific parameters by our numeric results that in the last case

$$\mu_{\text{hop}}(T) \sim T^{-\kappa} \exp(-\varepsilon_a/T), \tag{2}$$

where $\kappa = 1$ ($\kappa = 3/2$) for adiabatic $\omega_0 \ll t$ (nonadiabatic $\omega_0 \gg t$) cases. Here, the activation energy ε_a is

$$\varepsilon_a = E_b/2 - t', \tag{3}$$

where E_b is the polaron binding energy, i.e., the renormalization of the lowest energy level due to the electron-phonon coupling and $t' = t$ ($t' = 0$) in the adiabatic (antiadiabatic) case. The hopping transport begins above a temperature that has been derived to lie in the range between $\omega_0/4$ and $\omega_0/2$ [20,25]. As we found in our studies, at high enough temperatures, the mobility $\mu_\lambda(T)$ tends to saturate also at strong EPC. Moreover, at all couplings, weak or strong, the mobilities converge to close values that are almost independent of EPC λ, at least in the logarithmic scale.

It is worth discussing the evolution of $T_C(\lambda)$ and $T_D(\lambda)$ curves with the adiabaticity ω_0/t (note that the curves shown in Fig. 1 have been obtained at $\omega_0 = t$). By studying a more adiabatic case $\omega_0 = t/4$ (Supplemental Material [37]), we conclude that all the statements we put below for $\omega_0 = t$ do not change qualitatively for $\omega_0 = t/4$. The only changes in the schematic phase diagram (see arrows in Fig. 1) are the shift down of $T_C(\lambda)$ and $T_D(\lambda)$ governed by the decrease of $\omega_0/4$ and shift to the left dictated by the decrease of the critical EPC from $\lambda_c(\omega_0 = t) \approx 2$ to $\lambda_c(\omega_0 = t/4) \approx 1.1$ [see Figs. 2(b)–2(d)]. We conclude that the general properties are governed by the ratio $\omega_0/(4t)$ of the phonon frequency to the bandwidth $W = 4t$, which is similarly small for both cases. The Boltzmann constant k_B, a, t, $\hbar$, and e are set to unity throughout the Letter.

From weak to strong coupling regime.—Below, we present numeric data for the Holstein model at $\omega_0 = t$, if it is not stated otherwise. The goal is to get $\mu_\lambda(\omega, T)$ in the weak, intermediate, and strong EPC in a wide range of temperatures. The crossover from weak $\lambda \ll 1$ to strong $\lambda \gg 1$ regime is extremely smooth in one dimension [47,48]. So, we used the diagrammatic Monte Carlo method [8] to find the value of the coupling λ_c constant dividing these regimes and calculated the effective mass renormalization m^*/m_0, the binding energy E_b, and the mean number of phonons $\langle H_{\text{ph}} \rangle$ ($H_{\text{ph}} = \sum_k b_k^\dagger b_k$) in the phonon cloud of a single polaron [Figs. 2(b), 2(c), and 2(d)] at $T = 0$. The second derivatives $d^2\langle H_{\text{ph}} \rangle/d\lambda^2$ and $d^2(m^*/m_0)/d\lambda^2$ change signs at λ_c. Therefore, we define weak ($\lambda < \lambda_c$), intermediate ($\lambda \simeq \lambda_c$), and strong $\lambda > \lambda_c$ coupling regions. Also, the temperature dependence of the kinetic energy [Fig. 2(a)] suggests the same value for λ_c. Indeed, the average value of the kinetic energy $\langle -\hat{K}_{xx} \rangle$ is a monotonic (nonmonotonic) function of T at $\lambda < \lambda_c$ ($\lambda > \lambda_c$) with crossover value $\lambda_c \cong 2$ at $\omega_0 = t$ and $\lambda_c \cong 1$ at $\omega_0 = t/4$.

The transport properties.—In Fig. 3(a) we present $\mu_\lambda(T)$ in the perturbative ($\lambda = 0.01$), weak ($\lambda = 0.5$), intermediate

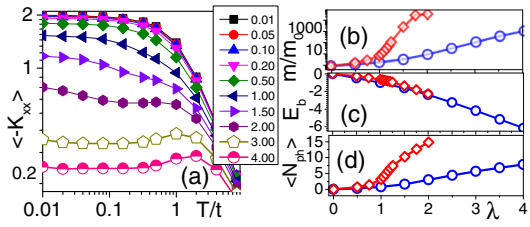

FIG. 2 (color online). Dependence of polaron properties on λ. (a) Temperature dependence of the kinetic energy for $\omega_0 = t$ (in units of t). Dependence at $T = 0$ of (b) the effective mass m^*/m_0, (c) the binding energy (in units of t), and (d) the mean number of phonons in the polaron cloud for $\omega_0 = t$ (circles) and $\omega_0 = t/4$ (diamonds).

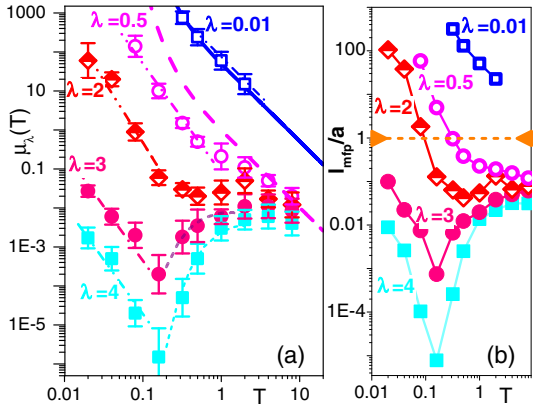

FIG. 3 (color online). Temperature dependence of mobility and MFP at $\omega_0 = t$. (a) dc mobility $\mu_\lambda(T)$ (in units of $ea^2/\hbar$). Unbiased numeric values at $\lambda = 0.01$ (open squares), $\lambda = 0.5$ (open circles), $\lambda = 2$ (semifilled diamonds), $\lambda = 3$ (filled circles), and $\lambda = 4$ (filled squares). Solid bold ($\lambda = 0.01$) and dashed bold ($\lambda = 0.5$) lines in the top part of the figure show the results obtained by the Boltzmann approach [49]. Fit of the mobility by the activation law Eqs. (2) and (3) is shown for $T > 0.2$ at $\lambda = 3$ (short-dash line) and $\lambda = 4$ (dotted line). Linear dash-dot-dot lines are fits of the low-temperature contribution of mobility, for all the values of λ, by a power law $\mu \sim T^{-\delta}$. (b) MFP, in units of the lattice parameter a, vs temperature [the symbols are the same as those used in panel (a)].

($\lambda = 2$), and strong ($\lambda = 3$ and 4) EPC limits. First, we show that we reproduce the Boltzmann result in the perturbative limit [compare the open squares and solid bold line in Fig. 3(a)]. Here, the physics is well described by a semiclassical picture; i.e., the MFP is much greater than the lattice parameter, and the motion remains coherent over a long distance before the electron is scattered. A perturbative low λ analytic treatment of the Holstein model predicts power laws (1) with $\delta = 3/2$ for $T \ll t$ and $\delta = 2$ for $T \gg t$ [22]. Our data [dash-dot line fitting positions of the open squares in Fig. 3(a)] in the range $0.32 < T < 2$ support the value $\delta = 2$. We restricted our analysis to $T > 0.3$ at $\lambda = 0.01$ because of the instability of the spectral analysis for extremely narrow ($< 10^{-3}$) and high ($> 10^3$) Drude peaks (Supplemental Material [37]).

The Boltzmann (bold dashed line) and unbiased (open circles) results are already different at $\lambda = 0.5$ [Fig. 3(a)]. Actually, for larger couplings, $\lambda \geq 0.5$, one can always fit $\mu_\lambda(T)$ by a power law (1) below some λ-dependent temperature $T_D(\lambda)$: $T_D(\lambda = 0.5) \approx 0.5$ and $T_D(\lambda \geq 2) \approx 0.25$. However, the index of the power law is different from $\delta = 2$ found in the perturbative $\lambda \ll 1$ limit. The best fit provides $\delta \approx 2.8$ for $\lambda = 0.5, 3, 4$ and $\delta \approx 3.2$ for $\lambda = 2$ [dash-dot-dot lines fitting low-temperature positions of open circles, diamonds, filled circles, and filled squares in Fig. 3(a)]. Our result is consistent with an exponent $3/2 \lesssim \delta \lesssim 3$ that is experimentally observed in many different materials [28,29,50–57]. We emphasize that the $d\mu_\lambda(T)/dT < 0$ behavior at low temperatures cannot be regarded as a proof of weak EPC.

For $T > T_D(\lambda)$, one can observe mobility saturation at $\lambda \leq 2$ whereas, at $\lambda = 3, 4$, hopping transport followed by mobility saturation. In particular, the hopping transport is naturally distinguished from the resistivity saturation regime by the existence of a temperature range with positive derivative $d\mu_\lambda(T)/dT > 0$ above a characteristic temperature whose analytical estimate is in the range between $\omega_0/4$ and $\omega_0/2$ [20,25]. We get a value consistent with $\approx\omega_0/4$ [filled circles and filled squares for mobilities at $\lambda = 3$ and 4 in Fig. 3(a)]. The analytic value of the activation energy ε_a of the activation law (2) is related to the binding energy of polaron E_b in Eq. (3). Inserting the binding energy of the polaron $E_b = 4.19$ ($E_b = 6.14$) at $\lambda = 3$ ($\lambda = 4$) into Eq. (3), one obtains $\varepsilon_a = 1.1$ ($\varepsilon_a = 2.07$), which is very close to the value 1.2 (2.1) obtained by the fit of $\mu_\lambda(T > 0.3)$ at $\lambda = 3$ ($\lambda = 4$) [see short-dash (dotted) line fitting the high-temperature dependence of filled circles (squares) in Fig. 3(a)]. Note that the fit is consistent only with the estimate of the activation energy in Eq. (3) corresponding to the adiabatic regime.

The mean free path.—So far, our analysis can distinguish a low-T regime at $T < T_D(\lambda)$, where power-law decrease of mobility is observed and, at $T > T_D(\lambda)$, two different regimes depending on temperature and EPC. However, it is clear that low-T regimes must be different at $\lambda \ll 1$ and $\lambda \gg 1$ because an increase of λ must eventually encounter the Mott-Ioffe-Regel limit for MFP $\ell_{\rm MFP}$ where band conduction with $\ell_{\rm MFP} > a$ changes to an incoherent metallic transport with $\ell_{\rm MFP} < a$. To estimate the MFP $\ell_{\rm MFP}$, we write the optical absorption $\sigma(\omega) = -i\langle \hat{K}_{xx} \rangle / [\omega + iM(\omega)]$ in terms of the memory function $M(\omega)$ [58,59]. At $\omega = 0$, the function M is real and determines the reciprocal of the optical relaxation time $1/\tau_r$ so that the mobility turns to be $\mu = -\langle \hat{K}_{xx} \rangle \tau_r$. This last relation allows us to extract τ_r, an important characteristic of equilibrium and even nonequilibrium [60] polaron dynamics. The MFP is defined by $\ell_{\rm MFP} = v\tau_r$, and a rough estimate of the average velocity v can be obtained by $v \simeq \sqrt{\langle \hat{j}(0)\hat{j}(0) \rangle}$. In Fig. 3(b) we plot the temperature dependence of $\ell_{\rm MFP}$ at the different values of λ.

As shown above, analysis of our data distinguish four regimes. Two low-T regimes, band conduction and incoherent metallic transport, are characterized by the power-law decrease of mobility when T increases. These two regimes are distinguished by the MFP, which is much larger than the lattice constant in the first case and much smaller than a in the second case. They are separated from the two high-T regimes by λ-dependent temperature $T_D(\lambda)$, where the metallic temperature dependence of mobility significantly changes. It becomes slower in the high-temperature saturation regime that sets up above $T_D(\lambda)$ at $\lambda \leq \lambda_c$. To the contrary, $\mu_\lambda(T)$ starts to increase with temperature at large EPC $\lambda > \lambda_c$, although it also eventually saturates at large T. Careful analysis of the frequency-dependent mobility $\mu_\lambda(\omega, T)$ shows that $T_D(\lambda)$ separates profoundly different

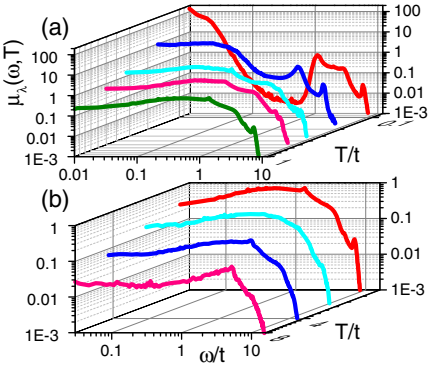

FIG. 4 (color online). Dynamic mobility (in units $ea^2/\hbar$) at $\omega_0 = t$ and $\lambda = 0.5$ at (a) low ($T = 0.08, 0.16, 0.32, 0.5, 1$) and (b) high ($T = 1, 2, 4, 8$) temperatures.

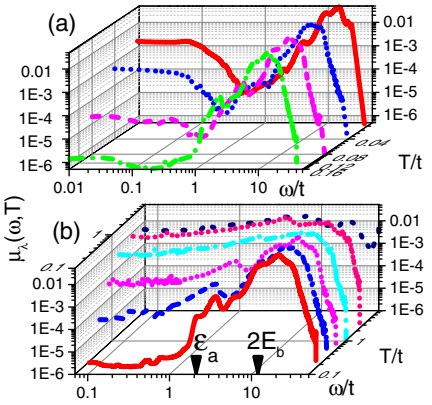

FIG. 5 (color online). Dynamic mobility (in units $ea^2/\hbar$) at $\omega_0 = t$ and $\lambda = 4$ at (a) low ($T = 0.02, 0.04, 0.08, 0.16$) and (b) high ($T = 0.16.0.32, 0.5, 1, 2, 8$) temperatures. Note opposite direction of T axis in (a) and (b). Arrows in the bottom of the figure show the activation energy ε_a from Eq. (3) and twice the polaron binding energy $2E_b$, respectively.

physical regimes. Namely, the DLP centered at $\omega = 0$ is observed only below $T_D(\lambda)$. This peak is explained by Drude theory, which assumes a single constant scattering rate and leads to $\mu(\omega)$ described by a Lorentzian centered at $\omega = 0$; i.e., a Bloch picture can be invoked. In any case, the weight of this peak decreases by increasing EPC and temperature and becomes negligible above $T_D(\lambda)$ where full incoherent motion sets in; i.e., the real space description becomes crucial and the Bloch picture breaks down. We note that the temperature $T_D(\lambda)$, where the DLP disappears, coincides with the temperature where conductivity saturation starts or with the temperature where the activated hopping regime arises [20,25].

Figure 4 shows temperature dependence of the $\mu_\lambda(\omega, T)$ in the weak EPC, $\lambda = 0.5$. The low-energy Drude peak is clearly seen at low T, $T \leq 0.16$, it almost vanishes at $0.32 < T < 0.5$, and it is absent for $T > 0.5$. The mobility in the band conduction regime quickly decreases with temperature at $T < 0.32$, which coincides with the temperature range of the Drude peak existence. For higher temperatures, in agreement with assumptions made in Refs. [61–64], the resistivity saturation occurs. Furthermore, we found that the Drude peak at $\lambda = 0.5$ and $T < 0.32$ gradually disappears without significant change of the high-energy part, which is again in complete agreement with Refs. [61–64].

The T dependence of the $\mu_\lambda(\omega, T)$ at strong EPC, $\lambda = 4$ (Fig. 5), also supports the statement that the large negative derivative $d\mu_\lambda(T)/dT < 0$ is associated with the presence of a DLP. Indeed, $d\mu_\lambda(T)/dT < 0$ at $T \leq 0.16$ (Fig. 3), which is just the range where DLP is seen [Fig. 5(a)]. As previously discussed, this regime is not related to a coherent band conduction transport, but it stems from an incoherent motion of the charge carriers with short MFP. To the contrary, a DLP is absent [Fig. 5(b)] in the domain of the thermally activated transport, $T \geq 0.25$ (Fig. 3). It is known [65] and confirmed in our study that the OC is characterized by a broad peak with the maximum around twice the binding energy [Fig. 5(b)]. At $0.25 < T < 2$, we find that $\mu_\lambda(\omega, T)$ is T independent at $\omega > \varepsilon_a$ while the spectral weight at $\omega < \varepsilon_a$ growth exponentially when T increases [Fig. 5(b)]. Then, the spectral weight starts to spread to larger frequencies when $T > 2$ and, as a result, the static mobility $\mu_\lambda(T)$ starts to saturate.

Conclusions.—We presented for the first time unbiased results for the temperature dependence of the optical conductivity $\sigma_\lambda(\omega, T)$ [or dynamic mobility $\mu_\lambda(\omega, T)$)] and static mobility $\mu_\lambda(T)$ of the one-dimensional Holstein polaron. The transport features display a strong λ and T dependence. In particular, we proved that a low-T power-law behavior exists until the DLP in the OC disappears at $T_D(\lambda)$. However, while the standard bandlike transport is recovered at weak couplings, an unconventional incoherent regime is observed at larger couplings. Moreover, at $T > T_D(\lambda)$, the μ-saturation (activated hopping transport) phenomenon occurs at weak (strong) couplings. Finally, our data imply that although mobilities and MFPs at different values of λ differ by many orders of magnitude at small temperatures, their values at $T > 4t$ become very close to each other (Fig. 3). Namely, regardless of the strength of the EPC, the effective scattering of a polaron turns out to be very strong when the temperature exceeds the bare bandwidth $4t$.

N. N. is supported by Grants-in-Aid for Scientific Research (S) (No. 24224009) from the Ministry of Education, Culture, Sports, Science and Technology (MEXT) of Japan and Strategic International Cooperative Program (Joint Research Type) from the Japan Science and Technology Agency. This work was funded by the ImPACT Program of the Council for Science, Technology and Innovation (Cabinet Office, Government of Japan).

[1] *Polarons in Advanced Materials*, edited by S. A. Alexandrov (Canopus/Springer, Bristol, 2007).
[2] R. P. Feynman, R. W. Hellwarts, C. K. Iddings, and P. M. Platzman, Phys. Rev. **127**, 1004 (1962).

[3] F. Ortmann, F. Bechstedt, and K. Hannewald, Phys. Rev. B **79**, 235206 (2009).
[4] A. S. Mishchenko, Usp. Fiz. Nauk **179**, 1259 (2009) [Sov. Phys. Usp. **52**, 1193 (2009)].
[5] A. H. Romero, D. W. Brown, and K. Lindenberg, J. Chem. Phys. **109**, 6540 (1998); A. H. Romero, D. W. Brown, and K. Lindenberg, Phys. Rev. B **59**, 13728 (1999); V. Cataudella, G. De Filippis, and G. Iadonisi, Phys. Rev. B **60**, 15163 (1999); O. S. Barisic, Phys. Rev. B **65**, 144301 (2002).
[6] M. Zoli, Phys. Rev. B **61**, 14523 (2000) and references therein.
[7] M. Berciu, Phys. Rev. Lett. **97**, 036402 (2006).
[8] A. S. Mishchenko, N. V. Prokof'ev, A. Sakamoto, and B. V. Svistunov, Phys. Rev. B **62**, 6317 (2000).
[9] A. S. Mishchenko, N. Nagaosa, N. V. Prokof'ev, A. Sakamoto, and B. V. Svistunov, Phys. Rev. Lett. **91**, 236401 (2003).
[10] G. De Filippis, V. Cataudella, A. S. Mishchenko, C. A. Perroni, and J. T. Devreese, Phys. Rev. Lett. **96**, 136405 (2006).
[11] A. S. Mishchenko, N. Nagaosa, Z.-X. Shen, G. De Filippis, V. Cataudella, T. P. Devereaux, C. Bernhard, K. W. Kim, and J. Zaanen, Phys. Rev. Lett. **100**, 166401 (2008).
[12] G. L. Goodvin, A. S. Mishchenko, and M. Berciu, Phys. Rev. Lett. **107**, 076403 (2011).
[13] G. De Filippis, V. Cataudella, A. S. Mishchenko, and N. Nagaosa, Phys. Rev. B **85**, 094302 (2012).
[14] J. Bonča, S. A. Trugman, and I. Batistić, Phys. Rev. B **60**, 1633 (1999).
[15] J. Loos, M. Hohenadler, A. Alvermann, and H. Fehske, J. Phys. Condens. Matter **19**, 236233 (2007).
[16] L. Vidmar, J. Bonča, and S. A. Trugman, Phys. Rev. B **82**, 104304 (2010).
[17] O. S. Barisic, Phys. Rev. B **69**, 064302 (2004).
[18] E. Jeckelmann and S. R. White, Phys. Rev. B **57**, 6376 (1998).
[19] A. Weiße, G. Wellein, A. Alvermann, and H. Fehske, Rev. Mod. Phys. **78**, 275 (2006).
[20] T. Holstein, Ann. Phys. (N.Y.) **8**, 343 (1959).
[21] L. Friedman and T. Holstein, Ann. Phys. (N.Y.) **21**, 494 (1963).
[22] S. H. Glarum, J. Phys. Chem. Solids **24**, 1577 (1963).
[23] D. C. Langreth and L. P. Kadanoff, Phys. Rev. **133**, A1070 (1964).
[24] L. Friedman, Phys. Rev. **133**, A1668 (1964).
[25] L. Friedman, Phys. Rev. **135**, A233 (1964).
[26] L. Friedman, Phys. Rev. **140**, A1649 (1965).
[27] D. C. Langreth, Phys. Rev. **159**, 717 (1967).
[28] L. Giuggioli, J. D Andersen, and V. M. Kenkre, Phys. Rev. B **67**, 045110 (2003).
[29] Y. C. Cheng, R. J. Silbey, D. A. da Silva Filho, J. P. Calbert, J. Cornil, and L. Brédas, J. Chem. Phys. **118**, 3764 (2003).
[30] A. Troisi and G. Orlandi, Phys. Rev. Lett. **96**, 086601 (2006).
[31] J.-F. Chang, H. Sirringhaus, M. Giles, M. Heeney, and I. McCulloch, Phys. Rev. B **76**, 205204 (2007).
[32] S. Fratini and S. Ciuchi, Phys. Rev. Lett. **103**, 266601 (2009).
[33] F. Ortmann, F. Bechstedt, and K. Hannewald, J. Phys. Condens. Matter **22**, 465802 (2010).
[34] V. Cataudella, G. De Filippis, and C. A. Perroni, Phys. Rev. B **83**, 165203 (2011).
[35] L. Vidmar, J. Bonča, M. Mierzejewski, P. Prelovšek, and S. A. Trugman, Phys. Rev. B **83**, 134301 (2011).
[36] The regime of *exponentially large mobility*, well known from early analytic studies [27], sets in at very low T. However, our numerical studies, as well as a real-time dynamics simulation method [35], could not reach such a regime.
[37] See the Supplemental Material http://link.aps.org/supplemental/10.1103/PhysRevLett.114.146401, which includes Refs. [38–45]. It contains a discussion on the mobility in the adiabatic case, a detailed description of the method used to extract mobility, and the estimation of the error bars.
[38] A. J. Millis, J. Hu, and S. Das Sarma, Phys. Rev. Lett. **82**, 2354 (1999).
[39] S. Fratini and S. Ciuchi, Phys. Rev. Lett. **91**, 256403 (2003).
[40] O. Gunnarsson, M. W. Haverkort, and G. Sangiovanni, Phys. Rev. B **82**, 165125 (2010).
[41] A. S. Mishchenko, *Correlated Electrons: From Models to Materials*, edited by E. Pavarini, W. Koch, F. Anders, and M. Jarrel (Forschungszentrum Julich GmbH, Julich, 2012), pp. 14.1–14.28.
[42] A. N. Tikhonoff and V. Y. Arsenin, *Solutions of Ill-Posed Problems* (Winston and Sons, Washington, DC, 1977).
[43] M. Jarrell and J. E. Gubernatis, Phys. Rep. **269**, 133 (1996).
[44] K. Vafayi and O. Gunnarsson, Phys. Rev. B **76**, 035115 (2007).
[45] A. W. Sandvik, Phys. Rev. B **57**, 10287 (1998).
[46] D. Emin, Phys. Rev. B **43**, 11720 (1991).
[47] L.-C. Ku, S. A. Trugman, and J. Bonca, Phys. Rev. B **65**, 174306 (2002).
[48] J. P. Hague, P. E. Kornilovitch, A. S. Alexandrov, and J. H. Samson, Phys. Rev. B **73**, 054303 (2006).
[49] G. De Filippis, V. Cataudella, A. de Candia, A. S. Mishchenko, and N. Nagaosa, Phys. Rev. B **90**, 014310 (2014).
[50] K. C. Kao and W. Hwang, *Electrical Transport in Solids* (Pergamon, New York, 1981).
[51] O. D. Jurchesku, J. Baas, and T. T. M. Palstra, Appl. Phys. Lett. **84**. 3061 (2004).
[52] C. D. Dimitrakopoulos and D. J. Mascaro, IBM J. Res. Dev. **45**, 11 (2001).
[53] H. Klauk, D. J. Gundlach, J. A. Nichols, and T. N. Jackson, IEEE Trans. Electron Devices **46**, 1258 (1999).
[54] W. Warta and N. Karl, Phys. Rev. B **32**, 1172 (1985).
[55] S. Nelson, Y. Lin, D. Gundlach, and T. N. Jackson, Appl. Phys. Lett. **72**, 1854 (1998).
[56] N. Karl, *Organic Electronic Materials*, edited by R. Farchioni and G. Grosso (Springer-Verlag, Berlin, 2001), pp. 283–326.
[57] M. E. Gershenson, V. Podzorov, and A. F. Morpurgo, Rev. Mod. Phys. **78**, 973 (2006).
[58] H. Mori, Prog. Theor. Phys. **33**, 423 (1965).
[59] H. Mori, Prog. Theor. Phys. **34**, 399 (1965).
[60] D. Golez, J. Bonča, L. Vidmar, and S. A. Trugman, Phys. Rev. Lett. **109**, 236402 (2012).
[61] O. Gunnarsson, M. Calandra, and J. E. Han, Rev. Mod. Phys. **75**, 1085 (2003).
[62] O. Gunnarsson and J. E. Han, Nature (London) **405**, 1027 (2000).
[63] M. Calandra and O. Gunnarsson, Phys. Rev. Lett. **87**, 266601 (2001).
[64] M. Calandra and O. Gunnarsson, Phys. Rev. B **66**, 205105 (2002).
[65] D. Emin, Phys. Rev. B **48**, 13691 (1993).